1736–1744 *Nucleic Acids Research, 1997, Vol. 25, No. 9*

Superhelix dimensions of a 1868 base pair plasmid determined by scanning force microscopy in air and in aqueous solution

Karsten Rippe*, Norbert Mücke and Jörg Langowski

Deutsches Krebsforschungszentrum, Abteilung Biophysik der Makromoleküle, Im Neuenheimer Feld 280, D-69120 Heidelberg, Germany

Received January 22, 1997; Revised and Accepted March 7, 1997

ABSTRACT

We have used scanning force microscopy (SFM) to study the conformation of a 1868 base pair plasmid (p1868) in its open circular form and at a superhelical density of $\sigma = -0.034$. The samples were deposited on a mica surface in the presence of $MgCl_2$. DNA images were obtained both in air and in aqueous solutions, and the dimensions of the DNA superhelix were analysed. Evaluation of the whole plasmid yielded average superhelix dimensions of 27 ± 9 nm (outer superhelix diameter *D*), 107 ± 51 nm (superhelix pitch *P*), and 54 ± 8° (superhelix pitch angle α). We also analysed compact superhelical regions within the plasmid separately, and determined values of *D* = 9.2 ± 3.3 nm, *P* = 42 ± 13 nm and $\alpha = 63 \pm 20°$ for samples scanned in air or rehydrated in water. These results indicate relatively large conformation changes between superhelical and more open regions of the plasmid. In addition to the analysis of the DNA superhelix dimensions, we have followed the deposition process of open circular p1868 to mica in real time. These experiments show that it is possible to image DNA samples by SFM without prior drying, and that the surface bound DNA molecules retain some ability to change their position on the surface.

INTRODUCTION

Negative supercoiling is an important feature of the DNA conformation of almost all prokaryotes and eukaryotes. Changes in the degree of supercoiling can have severe effects on the viability of a given organism because DNA supercoiling and various DNA associated processes are tightly interrelated [reviewed in (1)]. For example, DNA supercoiling has been shown to be connected with DNA transcription in several aspects: (i) negative supercoiling can facilitate the melting of the DNA at the transcription start site and thereby stimulate transcriptional activity [e.g. (2,3)], (ii) the transcription process itself leads to the generation of some negative supercoiling behind the polymerase and positive supercoiling in front of the polymerase [reviewed in (4)] and (iii) DNA supercoiling changes the DNA tertiary structure and can thereby facilitate interactions over large distances between regulatory proteins bound at enhancer sites and the promoter as discussed in ref. (5). DNA supercoiling is of similar relevance to other cases like replication or recombination [reviewed in (1)]. Accordingly, the characterization of the superhelical DNA conformation is important for the understanding of many DNA dependent biological processes.

Structural studies of superhelical DNA are constrained by the flexibility of the molecule. DNAs longer than ~50 nm (the persistence length) behave as flexible filaments, and their structure can only be characterized by average statistical properties. Furthermore, the conformation of the molecule becomes very sensitive to the environment, and processes such as drying and staining used in classical electron microscopy are prone to interfere with the structure determination. One way to circumvent this problem is to apply biophysical methods that characterize the structural properties of an ensemble of DNA molecules in solution, such as light scattering, ultracentrifugation or spectroscopic techniques. These methods are the least invasive way of studying the structure of large DNA molecules but they lack the possibility to observe structural details of single molecules.

Scanning force microscopy (SFM) (also termed atomic force microscopy or AFM) is an emerging technique that can be used for imaging DNA and other biomolecules without further fixing or staining, the only constraint being that the molecule is bound to a surface. SFM and its application for the study of biological macromolecules are described in several recent reviews (6–9) to which the reader is referred for additional information.

Preparation of the DNA sample for SFM imaging can be done by using Mg^{2+} to bind the DNA to the negatively charged surface of freshly cleaved mica. This process is relatively gentle and slow, and it has been shown that the DNA re-equilibrates on the substrate under the conditions of deposition used here (10). No further treatment is required to enhance the contrast and scanning is possible both in air and in liquid. Thus, the native hydration state of the DNA can be preserved and artefacts due to drying of the sample can be avoided. A disadvantage of SFM is that upon binding to the surface, the three-dimensional conformation of the DNA is constrained to two dimensions, and information on the orientation of the molecule in the third dimension is lost. In this

*To whom correspondence should be addressed. Tel: +49 6221 423392; Fax: +49 6221 423391; Email: Karsten.Rippe@dkfz-heidelberg.de

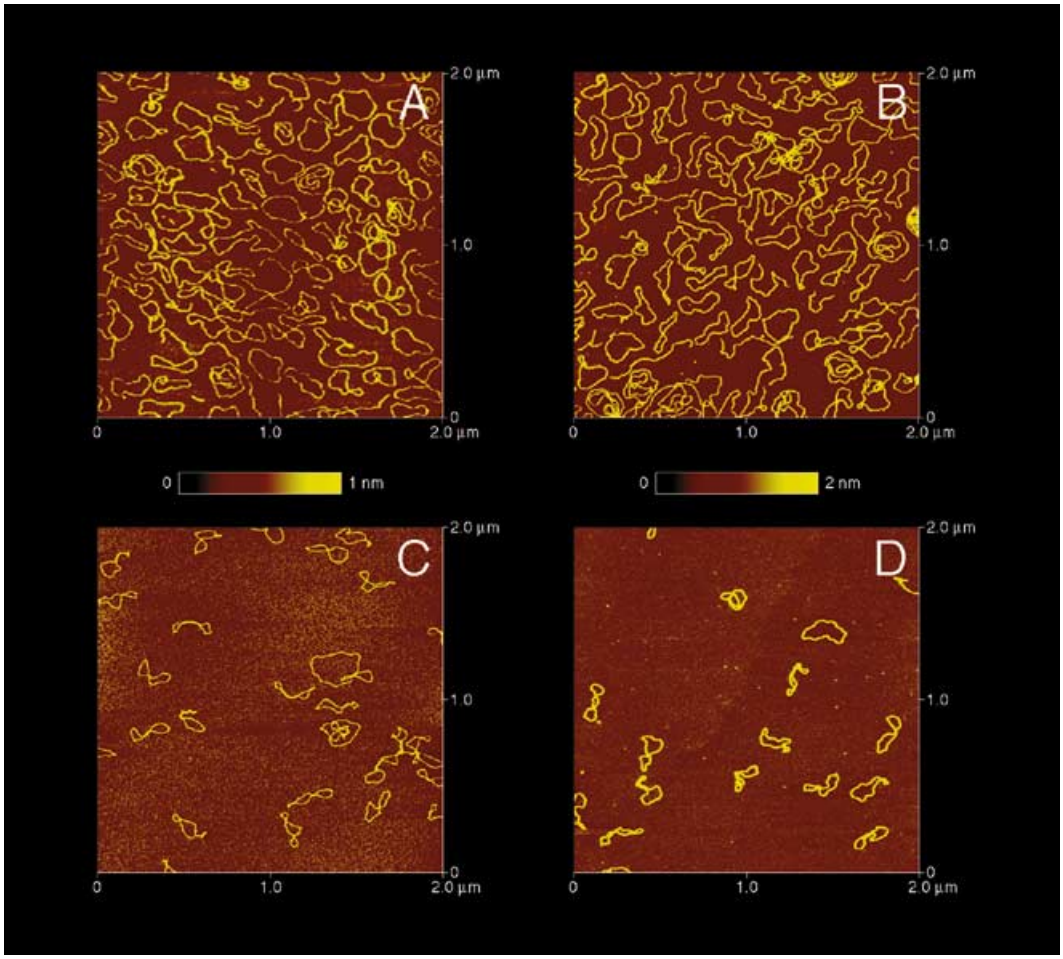

Figure 1. SFM images of plasmid p1868. (**A**) Open circular p1868 scanned in air. (**B**) Open circular p1868 scanned in water. (**C**) Superhelical p1868 scanned in air. (**D**) Superhelical p1868 scanned in water.

respect cryo-electron microscopy (cryo-EM) is advantageous as 3D images of DNA can be obtained from 3D reconstruction of stereo pair micrographs (11,12). Cryo-EM, however, also constrains the molecule into a 100 nm thin layer of ice, which is less than the extension of typical plasmid DNAs. In addition, it has been argued that the conformation of the DNA can change during the quick freezing process in cryo-EM (13). In summary, no single method can be relied on to give all necessary structural information about a flexible biopolymer, and SFM offers the possibility to gain complementary data on the conformation of single DNA molecules in near physiological conditions that are difficult to obtain by other methods.

Here we describe the use of SFM to study a small (1868 bp) superhelical plasmid at $\sigma = -0.034$ and its open circular form. A superhelical density around $\sigma = -0.03$ corresponds to the amount of negative supercoiling in *Escherichia coli* that is not constrained by bound proteins (14). Thus, the conformations of the superhelical molecules studied here are likely to be similar to those observed in the bacterial cell.

SFM has been used in a variety of studies of linear and circular DNA [e.g. (10,15-22)] and DNA–protein complexes [e.g. (23–26)]. The resolution of the SFM image is limited mostly by the size of the scanning tip, which typically has a tip curvature radius between 5 and 15 nm. With a curvature radius of 10 nm for a parabolic tip the theoretical resolution is 6.4 nm for objects of equal height (9). Thus, compared with the dimension of the DNA double helix, the tip is relatively large. This leads to a distortion of the true dimensions of the DNA in the SFM image. For example, with standard tips one usually observes an apparent width of ~10 nm for double-stranded DNA as compared with the known outer diameter of 2.37 nm for B-form DNA (27). In addition, interactions between the tip and the sample can occur, e.g. atomic repulsion between tip and sample or attractive capillary forces mediated by the thin water layer on the sample surface in ambient air (16,28). The latter artefact can be greatly reduced by scanning the sample not in air, but in liquid, a technique that has been considerably developed in recent years (22,29-34).

In this report we present images of superhelical and open circular plasmids. We show that high resolution images of DNA plasmids can be obtained both in air and in water and demonstrate how the superhelix dimensions can be determined from the SFM images.

MATERIALS AND METHODS

DNA plasmid p1868 is a derivative of pUC18 and was purified from *E.coli* HB 101 as described previously (35,36). Details on

the construction of the plasmid and the purification procedure are given elsewhere (Hammermann,M. *et al.*, manuscript submitted). Gel electrophoretic analysis showed that the superhelical fraction used here consisted of ~80% of topoisomers –6 corresponding to a superhelical density of $\sigma = -0.034$ in 40 mM Tris-acetate, pH 8.0 and 1 mM EDTA. In addition ~10% of the material was present as topoisomer –7 and another 10% was in the open circular form. The SFM images were obtained with a Nanoscope III (Digital Instruments, Santa Barbara, CA) operating in the 'tapping mode' following one of three different protocols:

Protocol I

DNA samples were prepared by deposition of 10 or 15 µl of a 2–5 nM DNA solution in 10 mM HEPES–KOH, pH 8.0, 10 mM $MgCl_2$ and 30 mM NaCl onto a piece of freshly cleaved mica (Plano GmbH, Wetzlar, Germany). The mica disc was washed immediately by dropping distilled water onto the surface and then drying the sample in a nitrogen stream. Images were recorded in air at ambient humidity using etched Si-probes (type Nanosensors) purchased from L.O.T. Oriel (Darmstadt, Germany) with a force constant 17–64 N/m, a thickness of 3.5–5.0 µm, a resonance frequency between 250 and 400 kHz and a tip curvature radius of ~10 nm (specifications given by the manufacturer).

Protocol II

The DNA samples were prepared as described in protocol I and the mica disc was mounted into the SFM liquid cell. Then the samples were rehydrated by injecting H_2O supplemented with 0.01% NP-40 into the liquid cell. Although not required, the presence of 0.01% NP-40 was found to facilitate the imaging process; stable images were usually obtained after 5–10 min. A buffer without 0.01% NP-40 (5 mM HEPES–KOH, pH 8.0, 2 mM $MgCl_2$) was also successfully used to rehydrate and image the samples (data not shown). Tapping in liquid was done with silicon cantilevers type ultralever from Park Scientific Instruments (Sunnyvale, CA) with a thickness of ~0.8 µm, using the C tip which has a typical force constant of 1 N/m, a tip curvature radius of 10 nm and a resonance frequency in air of ~140 kHz (specifications given by the manufacturer). For scanning in liquid a vibration frequency of ~20 kHz was usually used.

Protocol III

According to protocol I, a sample with a 6.8 kb open circular plasmid at a low DNA concentration was prepared so that only a few molecules per 4×4 µm scan were present. The sample was rehydrated in 5 mM HEPES–KOH, pH 8.0 buffer supplemented with 2 mM $MgCl_2$, and imaging was done as described in protocol II. After stable images of the 6.8 kb plasmid had been obtained, a solution of the much smaller open circular p1868 plasmid at a concentration of 4 nM was injected into the SFM liquid cell. After a few minutes of re-equilibration, images were recorded every ~3 min to follow the deposition process of the plasmid and to detect any rearrangements of DNA molecules on the surface. This protocol avoided drying of the DNA.

To determine the DNA double helix and the superhelix dimensions, 20 superhelical plasmids of images scanned in air (protocol I) and 20 molecules rehydrated in water (protocol II) were evaluated. Height, width and length measurements were made with the installed Nanoscope Software and with the program NIH image version 1.57. The dimensions of the superhelix were determined according to two strategies: the average dimensions of the superhelix were calculated according to the formalism described in ref. (37). In addition, direct SFM measurements were used to evaluate regions of the plasmid that showed a continuous plectonemic tract.

RESULTS

SFM images of the p1868 plasmid are displayed in Figures 1, 2 and 3. For the superhelical plasmids ($\sigma = -0.034$) in Figure 1C and D a 2×2 µm overview is presented, and in Figure 2C and D magnified images of single molecules are depicted. The open circular plasmids are shown in Figure 1A and B (overview), Figure 2A and B (magnification of single molecules), and in Figure 3 (time course demonstrating the binding to the surface). The images were made by using the three different protocols that are described under Materials and Methods.

According to protocol I, DNA images were obtained by scanning in air after deposition and drying the sample as described under Materials and Methods (Fig. 1A and C, Fig. 2A and C). In the presence of millimolar Mg^{2+} concentrations superhelical and open circular molecules bound efficiently to the freshly cleaved mica surface, and the protocol allowed fast and reliable imaging of DNA. However, a disadvantage of this method is that drying the sample could introduce conformation changes to the DNA as compared with its fully hydrated structure. The mean values for the apparent width and height for the DNA double helix were 10.0 ± 2.2 nm and 0.44 ± 0.07 nm (Table 1).

Table 1. Apparent dimensions of p1868 plasmid[a]

	Air (nm)	Water (nm)
Contour length, L_c	630 ± 12	640 ± 16
Axial rise per base pair[b]	0.34 ± 0.01	0.34 ± 0.01
DNA double helix width d' [c]	10.0 ± 2.2	10.8 ± 2.5
DNA double helix height	0.44 ± 0.07	1.14 ± 0.16
Superhelix maximal width D'_{max} [d]	16.1 ± 3.1	18.2 ± 5.9
Superhelix minimal width D'_{min} [d]	15.0 ± 4.0	16.9 ± 5.7
Superhelix maximal height[e]	0.86 ± 0.15	1.87 ± 0.28
Superhelix minimal height[e]	0.66 ± 0.13	1.41 ± 0.18

[a]Average values and standard deviations for 20 plasmid molecules measured in air or in water are given. Samples were prepared according to protocol I (air) or according to protocol II (water). Only molecules with two or more nodes were analysed, except for the determination of the DNA contour length which was done with the open circular plasmids.
[b]Calculated from the measured contour length and the number of base pairs (1868) of the plasmid studied.
[c]Apparent width of the DNA double helix measured at half maximum height.
[d]Superhelix width measured at half maximum height of the DNA double helix at the positions where the superhelix height had a minimum (D'_{max}) or a maximum (D'_{min}) (Fig. 4).
[e]Superhelix height measured at the maxima or the minima of the superhelix (Fig. 4).

In protocol II the samples were rehydrated in the microscope liquid cell by injecting H_2O supplemented with 0.01% NP-40 (Fig. 1B and D, Fig. 2B and D). Inasmuch as the conformational changes induced by the drying process are reversible, the

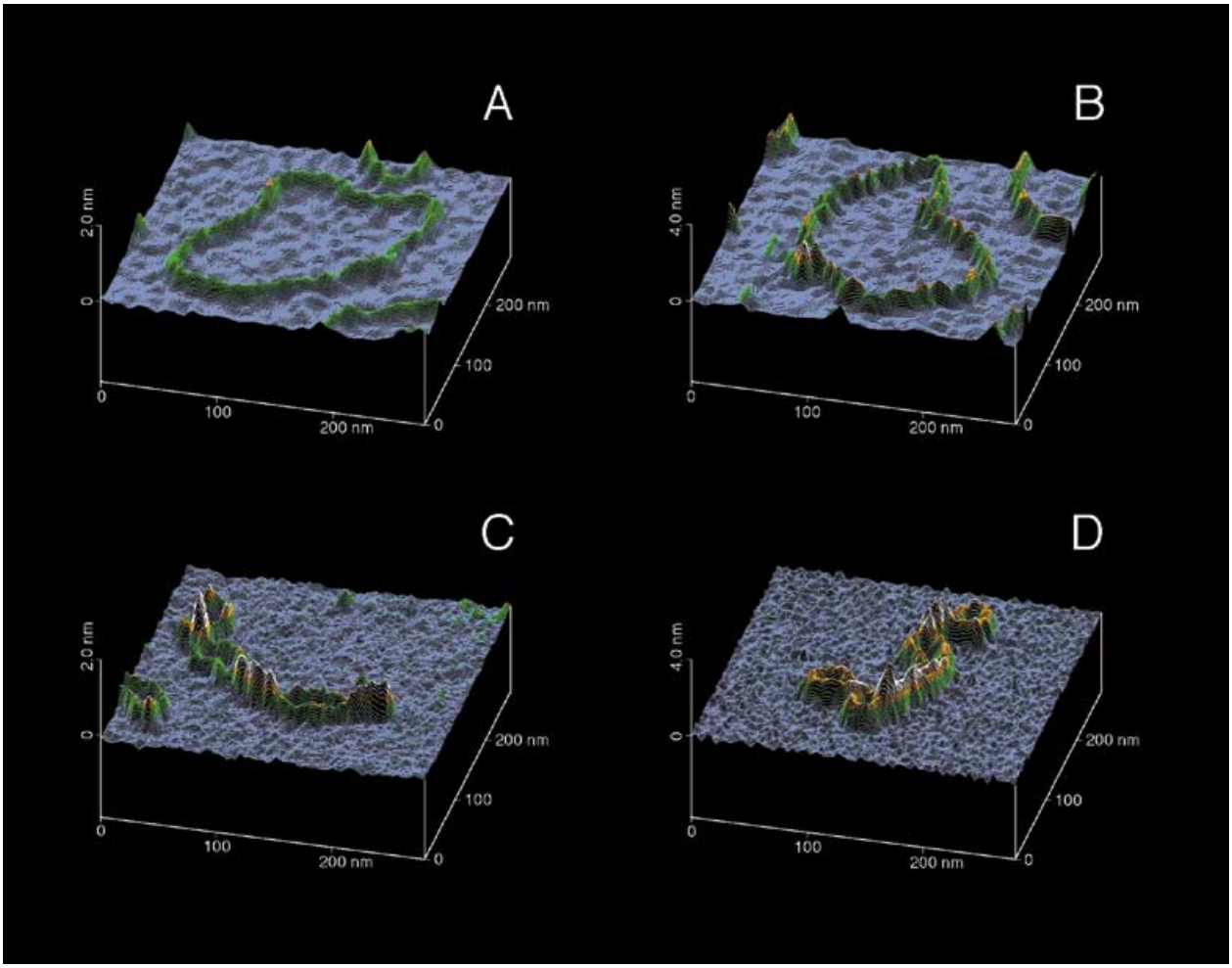

Figure 2. Line plot images of single plasmid molecules. (**A**) Open circular p1868 scanned in air. (**B**) Open circular p1868 scanned in water. (**C**) Superhelical p1868 scanned in air. (**D**) Superhelical p1868 scanned in water.

conformation of the molecules at native hydration should be restored under these conditions. The width of the DNA double helix (10.8 ± 2.5 nm) was similar to that measured in air, but the apparent height (1.14 ± 0.16 nm) was significantly larger (Table 1). The contour length of open circular plasmids in air and in water was 630 ± 12 and 640 ± 16 nm, respectively. This corresponds to an axial rise of 0.34 ± 0.01 nm/bp, characteristic for B-DNA under both conditions.

To determine the average superhelix dimensions over the whole plasmid we used the formalism described in ref. (37), which assumes that the DNA winds helically up and back down an imaginary capped cylinder with radius *r*. The length of this cylinder *l* (including the caps), the number of end loops *E* and the number of nodes *n* were measured on the SFM images. Then the superhelix radius *r* was calculated from *l*, *E*, *n* and the contour length L_c of the plasmid according to eqn 4 of ref. (37). The other parameters were derived as described in the legend to Table 2, where the results of this analysis are summarized. The average number of nodes *n* per molecule (and the value of *Wr* and Δ*Tw* derived from it) was somewhat higher in air (4.7 ± 1.9 nm) than in water (3.7 ± 1.3 nm), but for the other parameters there were no statistically significant differences at the 5% level between the measurements made in air and in water, as judged from a *t*-test of the means. The analysis according to ref. (37) of superhelical p1868 plasmid gave a superhelix radius *r* = 12.5 ± 4.7 nm, an outer diameter of *D* = 27 ± 9 nm, a superhelix pitch of *P* = 107 ± 51 nm and a pitch angle of α = 54 ± 8°. The calculated writhe was *Wr* = –3.4 ± 1.4 corresponding to Δ*Tw* = –2.6 ± 1.4 for Δ*Lk* = –6 (Table 2).

In addition to the analysis of the whole plasmid, we also analysed the tightly interwound parts of compact superhelical DNA regions separately. It has been pointed out in ref. (38) that the true width of a molecule in a closely packed array can be measured by SFM from the distance between adjacent minima or maxima. As shown in Figure 4B a similar argument can be made for the determination of the superhelix pitch. Although the dimensions of the tip will lead to a distortion of the true dimensions of the superhelix, the distance between two neighboring minima or maxima should be independent of the size of the tip, as long as it is small enough to resolve the changes of the superhelix height at all. From the measured distance between adjacent minima or maxima we determined a value of 41 ± 8 (air) and 42 ± 17 nm (rehydrated in water) for the length of one superhelical turn (Table 3).

Table 2. Average superhelix dimensions of p1868 plasmid[a]

	Air	Water	Air/water
Length of superhelix axis *l* (nm)[b]	246 ± 23	252 ± 22	249 ± 23
Number of nodes *n*[c]	4.7 ± 1.9	3.7 ± 1.3	4.2 ± 1.7
Number of end loops *E* [d]	2.0 ± 0.0	2.0 ± 0.0	2.0 ± 0.0
Superhelix radius *r* (nm)[e]	11.6 ± 4.4	13.6 ± 4.5	12.5 ± 4.7
Superhelix diameter *D* (nm)[f]	26 ± 9	30 ± 9	27 ± 9
Interstrand distance *z* (nm)[g]	21 ± 9	25 ± 9	23 ± 9
Superhelix pitch *P* (nm) [h]	95 ± 45	122 ± 54	107 ± 51
Pitch angle α (degree) [i]	52 ± 8	55 ± 8	54 ± 8
Δ*Lk* [j]	–6	–6	–6
Wr [k]	–3.7 ± 1.6	–3.0 ± 1.1	–3.4 ± 1.4
Tw [l]	–2.3 ± 1.6	–3.0 ± 1.1	–2.6 ± 1.4

[a]Values were determined as described in ref. (37) from the same set of superhelical molecules evaluated in Table 1. The analysis assumes that the DNA winds helically up and back down an imaginary capped cylinder with radius *r* and height *l*, and gives superhelix dimensions that are averaged over the whole molecule. The column to the right has the average values for both the samples measured in air and in water. An outer diameter of *d* = 2.4 nm for the B-DNA helix was used in the analysis (27).
[b]Length of superhelix axis *l* including the end loops [Fig. 3 of ref. (37)].
[c]Number of crossovers or nodes *n* of the superhelix.
[d]Number of end loops *E* of the plasmid molecule.
[e]The superhelix radius *r* was calculated according to eqn 4 from (37) by using the values of *l*, *n* and *E* determined from the SFM images and the contour length L_c = 635 nm of the plasmid.
[f]The outer superhelix diameter *D* was calculated from *r* according to $D = 2 \cdot r + d$.
[g]The separation distance *z* of the strands in the superhelix was calculated from *r* according to $z = 2 \cdot r - d$ (Fig. 4C).
[h]The superhelix pitch *P* is the length of one superhelical turn. It was calculated from *r* and α as described in ref. (37).
[i]The pitch angle α was calculated according to eqn 5 of ref. (37) from *l*, *E*, *r* and L_c.
[j]Determined from the gel electrophoretic analysis which showed that ~80% of the plasmid sample consisted of topoisomer –6.
[k]Determined from *n* and α according to the expression $Wr = -n \cdot \sin\alpha$ (49).
[l]Determined from $\Delta Lk = Wr + \Delta Tw$.

Table 3. Dimensions of superhelical regions within the p1868 plasmid[a]

	Air	Water	Air/water
Superhelix radius *r* (nm)[b]	3.1 ± 0.9	3.7 ± 2.2	3.4 ± 1.7
Superhelix diameter *D* (nm)[c]	8.5 ± 1.7	9.8 ± 4.3	9.2 ± 3.3
Interstrand distance *z* (nm)[d]	3.7 ± 1.7	5.0 ± 4.3	4.4 ± 3.3
Superhelix pitch *P* (nm)[e]	41 ± 8	42 ± 17	42 ± 13
Pitch angle α (degree)[f]	65 ± 14	61 ± 23	63 ± 20

[a]For the same set of superhelical molecules described in Tables 1 and 2 the superhelical regions within the plasmid were analysed separately.
[b]The superhelix radius was calculated from the interstrand distance *z* according to $r = 0.5 \cdot z + 0.5 \cdot d$.
[c]The outer superhelix diameter was calculated from $D = z + 2 \cdot d$.
[d]The separation distance *z* of the strands in the superhelix was calculated from $z = D'_{max} - d' - d$ (Fig. 4C). D'_{max} and d' are given in Table 1.
[e]The superhelix pitch *P* was determined from the measured distance between two neighbouring minima or two neighbouring maxima in the superhelix. The average value of this distance corresponds to the length of half a superhelical turn (Fig. 4B).
[f]The pitch angle α was determined from the superhelix pitch *P* and the superhelix radius *r*.

To determine the outer diameter *D* of the superhelix the dimensions of the scanning tip have to be accounted for. The images shown here were recorded with conventional commercially available tips with a tip radius of ~10 nm. As shown in Figure 4A, the relatively large size of the tip (as compared with the dimensions of the DNA double helix) leads to an apparent width d' that is too large for direct measurements of the DNA double helix diameter *d*. However, for two strands lying side by side the separation distance *z* between the two strands can be determined by subtracting d' from the measured width which equals $d' + d + z$ (Fig. 4A). Then *z* can be calculated with the known diameter of *d* = 2.4 nm for B-DNA. Along these lines we can estimate the distance *z* between two strands in the superhelix. The measured maximal height of the superhelix is 2 times (air) or 1.6 times (water) higher than that of the DNA double helix (Table 1). From this observation we conclude that at the position of maximal height the two DNA strands in the superhelix approach each other closely during the scanning process so that almost no space is left between them (see left side of Fig. 4C). Accordingly, we infer that at the point of the superhelix where the height is minimal and the width is maximal the two DNA strands lie side by side and both strands contact the surface during the scanning process, as depicted on the right side of Figure 4C. The path of the SFM tip is also affected somewhat by the neighboring higher regions of the superhelix as indicated in the cross-section. However, this should not change the measured value of D'_{max} significantly for

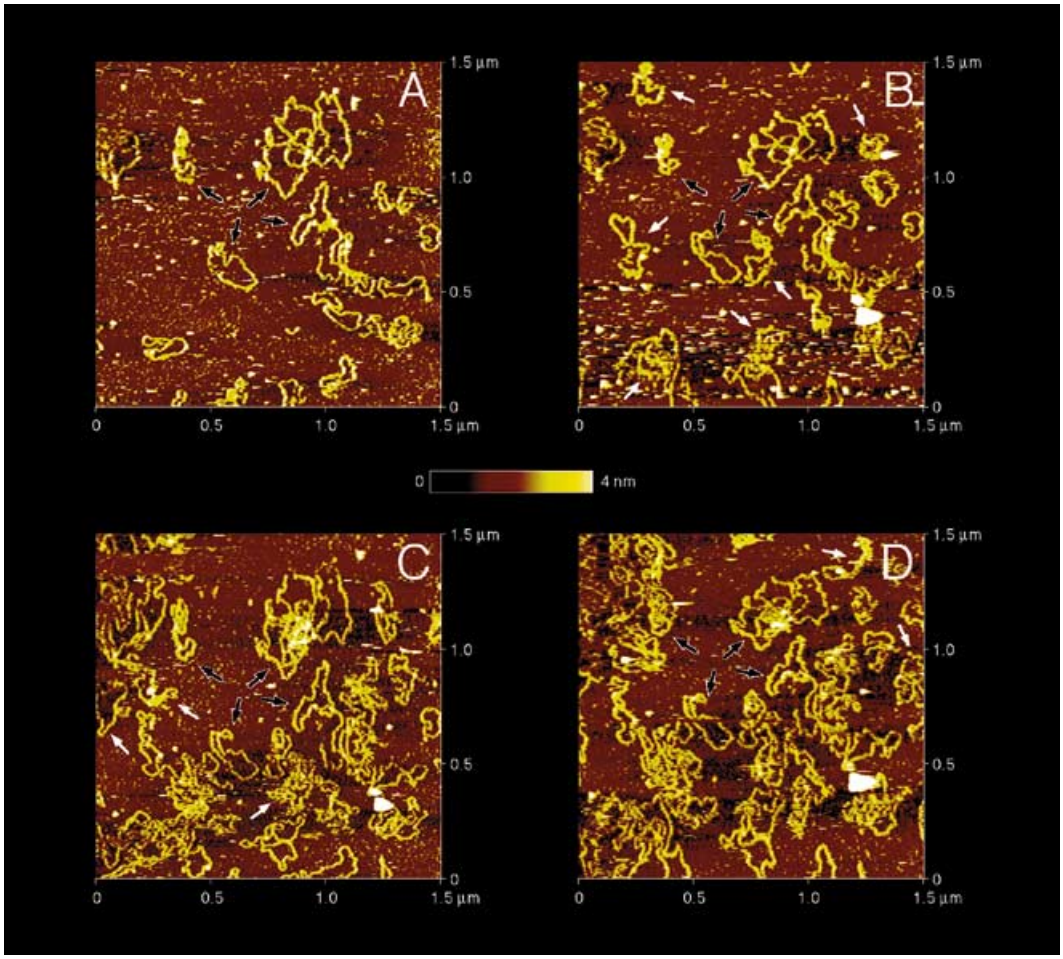

Figure 3. Time course of deposition of relaxed p1868 injected into the liquid cell. Images A–D were recorded sequentially at about 6 (**A**), 9 (**B**), 12 (**C**) and 15 min (**D**) after the sample of open circular p1868 had been injected into the liquid cell as described under Materials and Methods, protocol III. White arrows show newly appearing p1868 molecules from one image to the next. Black arrows indicate plasmid molecules that were present throughout the time course and show some rearrangement from one image to the next.

the present dimensions of tip and DNA superhelix. Thus, we can determine z from the measured maximal width of the superhelix D'_{max} by subtracting the apparent width of the DNA double helix d' and a value of d = 2.4 nm for the diameter of B-DNA. This yields values of $z = 3.7 \pm 1.7$ nm (air) and 5.0 ± 4.3 nm (water) (Table 3). A *t*-test analysis of the mean values determined for z, r, α, P and D in air and in water showed no significant differences at the 5% level, and the average values for all molecules are given in the right column of Table 3. For the compact superhelical regions of the p1868 plasmid a radius $r = 3.4 \pm 1.7$ nm, a diameter $D = 9.2 \pm 3.3$ nm, a superhelix pitch $P = 42 \pm 13$ nm, and a pitch angle $\alpha = 63 \pm 20°$ were determined.

In protocol III a solution of open circular p1868 DNA was injected directly into the SFM liquid cell containing a solution of 5 mM HEPES–KOH, pH 8.0 buffer with 2 mM $MgCl_2$ (Fig. 3A–D). This procedure completely avoided drying of the DNA. Inspecting successive images recorded at 6 (Fig. 3A), 9 (Fig. 3B), 12 (Fig. 3C) and 15 min (Fig. 3D) after injection of the plasmid, one can notice two important points: first, over time newly bound molecules are visible on the surface, indicated by white arrows. Secondly, molecules bound to the surface that are present in all four images (indicated by the black arrows) show some variation in their shape and position. This indicates that although the molecules are bound to the surface, they still have retained some ability for two dimensional diffusion.

DISCUSSION

We have studied the conformation of a 1868 bp long plasmid in its superhelical and in its open circular conformation. SFM images were recorded both in air and in aqueous solution and the DNA dimensions were analysed. The values determined here for the apparent width and height of the DNA double helix (Table 1) fall within the range obtained in other studies for DNA plasmids bound to a mica surface via Mg^{2+}. For imaging in air apparent widths of 12.3 ± 3.3 nm (16), 21.9 ± 3.7 nm (18) and 11.2 ± 1.8 nm (39) have been determined, and the height was measured to be 1.32 ± 0.34 nm (16), 0.79 ± 0.05 nm (18), 0.43 ± 0.08 nm (39) and 0.54 ± 0.12 nm (40). The dimensions of the DNA double helix in aqueous solution were found to be 19 ± 4 nm with a height of 2.5 ± 0.5 nm (41).

The apparent width of the DNA double helix is largely dependent on the size of the tip and this parameter therefore is not very meaningful in terms of the real DNA dimensions (Fig. 4A).

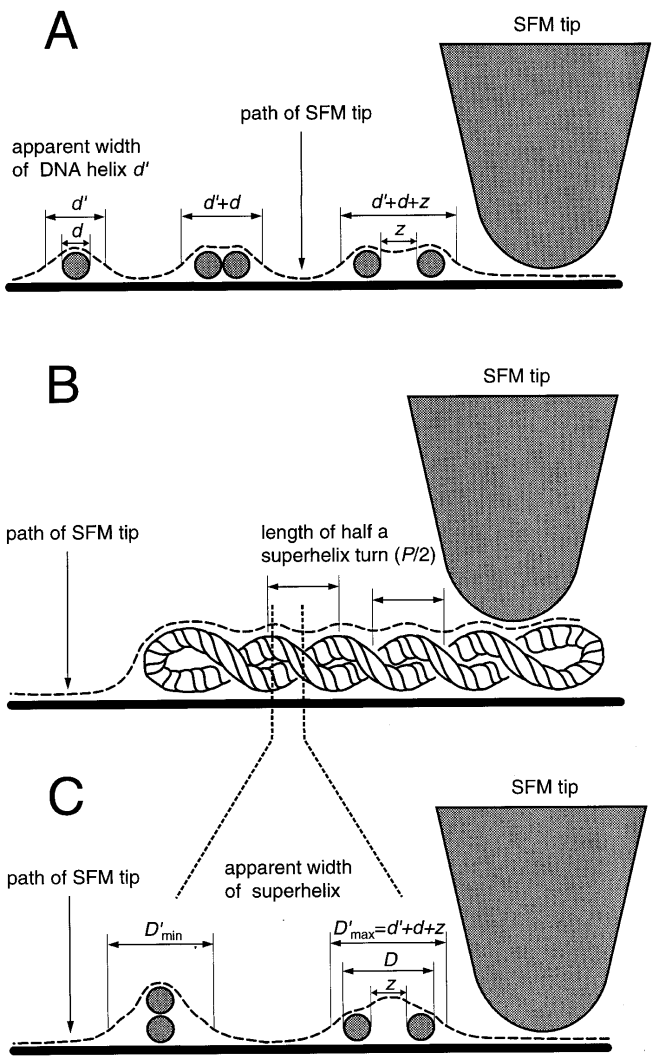

Figure 4. Analysis of compact superhelix regions within the plasmid by SFM. (**A**) Cross section through a DNA double helix (left), two DNA double helices lying side by side (middle) or two DNA double helices separated by a distance *z*. The apparent DNA width was measured at the half maximal height (full width at half maximum). Due to the size of the tip, the apparent diameter in the SFM image is much larger than the true DNA diameter which should be 2.4 nm for B-DNA. For the width of two DNA strands the separation distance *z* between the two strands can be determined by the width measured by SFM ($d' + d + z$) and then subtracting d' and d (= 2.4 nm). (**B**) Determination of superhelical pitch. The distance between two adjacent minima or two adjacent maxima corresponds to the length of half a superhelical turn which is half the superhelix pitch *P*. (**C**) Cross section through a superhelical region of the plasmid at the maximal (left) and minimal height (right) of the superhelix. The maximal width is measured at the points where the height is minimal and this value can be used to estimate the distance *z* between the two DNA strands that form the superhelix.

The low height for DNA imaged in air, 0.44 ± 0.07 nm instead of 2.4 nm expected for B-DNA, could result from two effects: compression of the molecule by the tip during the scanning process and attractive capillary forces mediated by the thin water layer on the sample surface which result in an apparent reduction of the DNA height. Both factors are likely to be different in water, which would explain the observed increase in the measured DNA height from 0.44 ± 0.07 to 1.14 ± 0.16 nm.

Drying the DNA sample can potentially introduce a conformation change. It is known that at low relative humidity (60–75%) natural DNA sequences will undergo a transition from B-DNA into the A-form. A-DNA is characterized by a different helix geometry and in particular by a shorter axial rise of 0.28 nm/bp instead of 0.34 nm/bp in B-DNA, as determined by X-ray diffraction of DNA fibres (42). One would therefore expect a shortening of the DNA contour, detectable in the SFM images, if a transition from B- to A-DNA occurs. Under the conditions studied here we found a helical rise of 0.34 ± 0.01 nm/bp characteristic for B-form DNA with both dried and rehydrated open circular plasmids. This is in agreement with the results from previous studies which reported 0.34 ± 0.01 nm (17,20,43). In addition, it was observed with samples deposited from aqueous buffers to mica that the characteristic B-DNA spacing of 0.34 ± 0.03 nm/bp persisted even in propanol (41). These results demonstrate that the binding of the plasmid DNA molecules to the mica surface can prevent the expected transition to the A-form under some conditions.

On the other hand, several studies reported lower helical rise values which would suggest that at least a partial transition to the A-form occurs: a helical rise between 0.28 and 0.33 nm was observed by Bustamante and co-workers for three different plasmids (16). Gold-labelled linear DNA molecules measured in air at a relative humidity <10% showed a helical rise of 0.28 nm/bp (40), and a value of 0.30 ± 0.01 nm/bp was determined by Thundat *et al.* (18). For a set of eight linear DNA fragments from 350 to 5994 bp Rivetti *et al.* (10) measured a helical rise of 0.312 ± 0.005 nm/bp. However, the authors attributed this discrepancy to the value for B-form DNA to the smoothing procedure applied in their image analysis program and to limitations in the pixel resolution. In a recent SFM study, Hansma *et al.* (19) estimated a value of 0.25 nm/bp for short linear DNA fragments (50, 100 and 200 bp), indicative of an A-DNA conformation. They suggested that the ability of mica-bound DNA strands to undergo a B- to A-transition will depend on the strength of the binding interaction between DNA and mica, which is expected to be higher with large DNA fragments (19,41). Thus, the varying results of contour length measurements of dried samples in air could reflect differences in the size of the DNA samples and/or the deposition protocol used for binding the DNA to mica.

The average dimensions of the superhelix can be determined from the contour length L_c, the measured length of the superhelix *l*, the number of nodes *n* and the number of end loops *E* as described in ref. (37). The values obtained here by SFM (outer superhelix diameter D = 27 ± 9 nm, superhelix radius r = 12.5 ± 4.7 nm, superhelical pitch P = 107 ± 51nm and superhelix pitch angle $\alpha = 54 \pm 8°$, at $\sigma = -0.034$, Table 2) can be compared with results of electron microscopy studies of superhelical plasmids (12,37,44). Boles *et al.* determined values of r = 9.6 nm, P = 99 nm and $\alpha = 59°$ for a 7 kb plasmid spread in TE buffer at $\sigma = -0.033$ (37). In another study cryo-electron microscopy was used to analyse pUC18 (2686 bp) at a somewhat higher σ of –0.047, and values of superhelix diameter D = 12 nm, P ≈ 55 nm and $\alpha = 55°$ were determined in TE buffer (44).

As judged from EM studies and from Brownian dynamics simulations ~75% of the linking number deficit $\Delta Lk = -6$ is expected to be in the writhe component *Wr* and 25% in the change of twist ΔTw (37,44–46). Here we determined a writhe of –3.7 ± 1.6 (air) and –3.0 ± 1.1 (water) corresponding to a change of twist of –2.3 ± 1.6 (air) and –3.0 ± 1.1 (water), respectively (Table 2). This

would suggest that the writhe contributes only 50–60% to ΔLk. It appears unlikely that the slight differences with respect to the solution conditions used for the determination of ΔLk on the gel (40 mM Tris-acetate, pH 8.0 and 1 mM EDTA) and the SFM sample deposition buffer (10 mM HEPES–KOH, pH 8.0, 10 mM $MgCl_2$ and 30 mM NaCl) would lead to the observed value of writhe (47). In addition, there is no evidence for a structural transition of the DNA induced by negative supercoiling from the gel electrophoretic analysis. Thus, the observed difference to the expected value of *Wr* are most likely due to the binding of the DNA to the surface, which might favour some redistribution of writhe and twist under the conditions used here. The somewhat less negative value of *Wr* determined in water might reflect an increased electrostatic repulsion in the rehydration solution (H_2O + 0.01% NP-40) as compared with the deposition conditions (10 mM HEPES–KOH, pH 8.0, 10 mM $MgCl_2$ and 30 mM NaCl, ionic strength 70 mM), which could lead to a further decrease of ΔTw. This would be in agreement with the observed dependence of the duplex winding on the ionic environment of the DNA (47). That some conformation rearrangement of the mica bound plasmids is possible in liquid can be seen with the DNA samples shown in Figure 3.

The above values are derived from an analysis that assumes an idealized regular conformation of the superhelix. However, in our studies we usually observe tightly interwound regions that alternate with more open regions of the plasmid, rather than a regular superhelix structure. Instead of averaging over the whole molecule, we therefore measured also the tightly interwound parts of these compact superhelical DNA regions separately, and obtained values of $D = 9.2 \pm 3.3$ nm, $r = 3.4 \pm 1.7$ nm, $P = 42 \pm 13$ nm and $\alpha = 63 \pm 20°$ (Table 3). These values are expected to be similar to the superhelix conformation that is formed throughout the whole plasmid molecules upon increasing the superhelical density in the presence of $MgCl_2$. This view is supported by the results from electron microscopy studies. For example, for the above mentioned 7 kb plasmid the superhelix dimensions averaged over the whole plasmid at $\sigma = -0.059$ in the presence of 10 mM $MgCl_2$ were found to change to $r = 5.8$ nm, $P = 52$ nm and $\alpha = 55°$ (37). By cryo-EM it has been observed that very compact superhelix structures form at $\sigma = -0.06$ in the presence of 100 mM NaCl or 10 mM $MgCl_2$ (12,44). The interpretation of these findings as close contact of DNA double helices in the interwound region, however, was recently challenged by solution measurements (13).

The quality of the images obtained by injection of the DNA (Fig. 3, protocol III) was not as good as with protocols I and II. This is likely to be related to the more difficult sample preparation and to the requirement to record successive images which leaves less possibilities to optimize the instrument settings. Nevertheless, the results show that one can image DNA molecules that have not been dried before, and therefore their native hydration state has been preserved throughout the preparation. This technique has been developed by Hansma and co-workers (31,33,34), albeit by using a somewhat different deposition protocol. In addition, we were able to follow the binding of DNA to the mica surface by SFM. Together with the observation that the DNA plasmid molecules bound to the surface have still retained some ability to change their position and their location on the surface, as has been observed previously (31,33), this reveals the exciting potential of SFM to follow dynamic processes in real time. This feature is going to be even more important for studies of proteins and their interaction with DNA. For it is known that drying of protein samples often leads to an irreversible loss of protein activity, and recent work in studies of *E.coli* RNA polymerase (32,48) demonstrates that the transcription process can be visualized by SFM.

ACKNOWLEDGEMENTS

We thank Katalin Tóth and Nathalie Brun for the p1868 plasmid samples. We are also grateful to Martin Guthold, Achim Schaper and Tom Jovin for their advice, to Helen Hansma for sharing preprints of their SFM work on DNA, to Alexandra Schulz for critical reading of the manuscript and to Ingrid Grummt for her support.

REFERENCES

1 Bates,A.D. and Maxwell,A. (1993) *DNA Topology*, Oxford University Press, Oxford.
2 Lamond,A.I. (1985) *EMBO J.*, **4**, 501–507.
3 Drew,H.R., Weeks,J.R. and Travers,A.A. (1985) *EMBO J.*, **4**, 1025–1032.
4 Wang,J.C. and Lynch,A.S. (1993) *Curr. Opin. Genet. Dev.*, **3**, 764–768.
5 Rippe,K., von Hippel,P.H. and Langowski,J. (1995) *Trends Biochem. Sci.*, **20**, 500–506.
6 Bustamante,C., Keller,D. and Yang,G. (1993) *Curr. Opin. Struct. Biol.*, **3**, 363–372.
7 Hansma,H.G. and Hoh,J.H. (1994) *Annu. Rev. Biophys. Biomol. Struct.*, **23**, 115–139.
8 Bustamante,C., Erie,D.A. and Keller,D. (1994) *Curr. Opin. Struct. Biol.*, **4**, 750–760.
9 Bustamante,C. and Rivetti,C. (1996) *Annu. Rev. Biophys. Biomol. Struct.*, **25**, 395–429.
10 Rivetti,C., Guthold,M. and Bustamante,C. (1996) *J. Mol. Biol.*, **264**, 919–932.
11 Dustin,I., Furrer,P., Stasiak,A., Dubochet,J., Langowski,J. and Egelman,E. (1991) *J. Struct. Biol.*, **107**, 15–21.
12 Bednar,J., Furrer,P., Stasiak,A., Dubochet,J., Egelman,E.H. and Bates,A.D. (1994) *J. Mol. Biol.*, **235**, 825–847.
13 Gebe,J.A., Delrow,J.J., Heath,P.J., Fujimoto,B.S., Stewart,D.W. and Schurr,J.M. (1996) *J. Mol. Biol.*, **262**, 105–128.
14 Bliska,J.B. and Cozzarelli,N.R. (1987) *J. Mol. Biol.*, **194**, 205–218.
15 Hansma,H.G., Vesenka,J., Siergerist,C., Kelderman,G., Morrett,H., Sinsheimer,R.L., Elings,V., Bustamante,C. and Hansma,P.K. (1992) *Science*, **256**, 1180–1184.
16 Bustamante,C., Vesenka,J., Tang,C.L., Rees,W., Guthold,M. and Keller,R. (1992) *Biochemistry*, **31**, 22–26.
17 Schaper,A., Pietrasanta,L.I. and Jovin,T.M. (1993) *Nucleic Acids Res.*, **21**, 6004–6009.
18 Thundat,T., Alison,D.P. and Warmack,R.J. (1994) *Nucleic Acids Res.*, **22**, 4224–4228.
19 Hansma,H.G., Revenko,I., Kim,K. and Laney,D.E. (1996) *Nucleic Acids Res.*, **24**, 713–720.
20 Coury,J.E., McFail-Isom,L., Williams,L.D. and Bottomley,L.A. (1996) *Proc. Natl. Acad. Sci. USA*, **93**, 12283–12286.
21 Samori,B., Siligardi,G., Quagliariello,C., Weisenhorn,A.L., Vesenka,J. and Bustamante,C.J. (1993) *Proc. Natl. Acad. Sci. USA*, **90**, 3598–3601.
22 Lyubchenko,Y.L. and Shlyakhtenko,L.S. (1997) *Proc. Natl. Acad. Sci. USA*, **94**, 496–501.
23 Erie,D.A., Yang,G., Schultz,H.C. and Bustamante,C. (1994) *Science*, **266**, 1562–1566.
24 Rees,W.A., Keller,R.W., Vesenka,G.Y. and Bustamante,C. (1993) *Science*, **260**, 1646–1649.
25 Pietrasanta,L.I., Schaper,A. and Jovin,T.M. (1994) *Nucleic Acids Res.*, **22**, 3288–3292.
26 Rippe,K., Guthold,M., von Hippel,P.H. and Bustamante,C. (1997) *J. Mol. Biol.* in press.
27 Dickerson,R.E., Drew,H.R., Conner,B.N., Kopka,M.L. and Pjura,P.E. (1983) *Cold Spring Harbor Symp. Quant. Biol.*, **47**, 13–24.
28 Thundat,T., Warmack,R.J., Alison,D.P., Bottomley,L.A., Lourenco,A.J. and Ferrel,T.L. (1992) *J. Vac. Sci. Technol. B*, **10**, 630–635.

29 Drake,B., Prater,C.B., Weisenhorn,A.L., Gould,S.A.C., Albrecht,T.R., Quate,C.F., Cannell,D.S., Hansma,H.G. and Hansma,P.K. (1989) *Science*, **243**, 1586–1589.
30 Hansma,P.K., Cleveland,J.P., Radmacher,M., Walters,D.A., Hillner,P., Bezanilla,M., Fritz,M., Vie,D., Hansma,H.G., Prater,C.B., Massie,J., Fukunaga,L., Gurley,J. and Elings,V. (1994) *Appl. Phys. Lett.*, **64**, 1738–1740.
31 Bezanilla,M., Drake,B., Nudler,E., Kashlev,M., Hansma,P.K. and Hansma,H.G. (1994) *Biophys. J.*, **67**, 2454–2459.
32 Guthold,M., Bezanilla,M., Erie,D.A., Jenkins,B., Hansma,H.G. and Bustamante,C. (1994) *Proc. Natl. Acad. Sci. USA*, **91**, 12927–12931.
33 Hansma,H.G., Laney,D.E., Revenko,I., Kim,K. and Cleveland,J.P. (1996) In Sarma,R.H. and Sarma,M.H. (eds) *Biological Structure and Dynamics*. Adenine Press, Albany, NY, pp. 249–258.
34 Hansma,H.G. and Laney,D.E. (1996) *Biophys. J.*, **70**, 1933–1939.
35 Kapp,U. and Langowski,J. (1992) *Anal. Biochem.*, **206**, 293–299.
36 Langowski,J. (1987) *Biophys. Chem.*, **27**, 263–271.
37 Boles,T.C., White,J.H. and Cozzarelli,N.R. (1990) *J. Mol. Biol.*, **213**, 931–951.
38 Hansma,H.G. (1995) *Biophys. J.*, **68**, 3–4.
39 Bezanilla,M., Manne,S., Laney,D.E., Lyubchenko,Y.L. and Hansma,H.G. (1995) *Langmuir*, **11**, 655–659.
40 Shaiu,W.L., Larson,D.D., Vesenka,J. and Henderson,E. (1993) *Nucleic Acids Res.*, **21**, 99–103.
41 Hansma,H.G., Bezanilla,M., Zenhausern,F., Adrian,M. and Sinsheimer,R.L. (1993) *Nucleic Acids Res.*, **21**, 505–512.
42 Leslie,A.G.W., Arnott,S., Chandrasekaran,R. and Ratliff,R.L. (1980) *J. Mol. Biol.*, **143**, 49–72.
43 Schaper,A., Starink,J.P.P. and Jovin,T.M. (1994) *FEBS Lett.*, **355**, 91–95.
44 Adrian,M., ten Heggeler-Bordier,B., Wahli,W., Stasiak,A.Z., Stasiak,A. and Dubochet,J. (1990) *EMBO J.*, **9**, 4551–4554.
45 Chirico,G. and Langowski,J. (1994) *Biopolymers*, **34**, 415–433.
46 Vologodskii,A.V. and Cozzarelli,N.R. (1994) *Annu. Rev. Biophys. Biomol. Struct.*, **23**, 609–643.
47 Anderson,P. and Bauer,W. (1978) *Biochemistry*, **17**, 594–601.
48 Kasas,S., Thomson,N.H., Smith,B.L., Hansma,H.G., Zhu,X., Guthold,M., Bustamante,C., Kool,E.T., Kashlev,M. and Hansma,P.K. (1997) *Biochemistry*, **36**, 461–468.
49 Fuller,F.B. (1971) *Proc. Natl. Acad. Sci. USA*, **68**, 815–819.